Shear viscosity in the postquasistatic approximation

C. Peralta, L. Rosales, B. Rodríguez-Mueller, and W. Barreto

August 2010

Publication Number: CSRCR2010-07

Computational Science & Engineering Faculty and Students Research Articles

Database Powered by the Computational Science Research Center Computing Group & Visualization Lab

COMPUTATIONAL SCIENCE & ENGINEERING

SAN DIEGO STATE UNIVERSITY

Computational Science Research Center
College of Sciences
5500 Campanile Drive
San Diego, CA 92182-1245
(619) 594-3430

PHYSICAL REVIEW D **81,** 104021 (2010)

Shear viscosity in the postquasistatic approximation

C. Peralta
Deutscher Wetterdienst, Frankfurter Str. 135, 63067 Offenbach, Germany[*]

L. Rosales
Laboratorio de Física Computacional, Universidad Experimental Politécnica "Antonio José de Sucre", Puerto Ordaz, Venezuela

B. Rodríguez-Mueller
Computational Science Research Center, College of Sciences, San Diego State University, San Diego, California, USA

W. Barreto
Centro de Física Fundamental, Facultad de Ciencias, Universidad de Los Andes, Mérida, Venezuela[†]
(Received 5 March 2010; published 10 May 2010)

We apply the postquasistatic approximation, an iterative method for the evolution of self-gravitating spheres of matter, to study the evolution of anisotropic nonadiabatic radiating and dissipative distributions in general relativity. Dissipation is described by viscosity and free-streaming radiation, assuming an equation of state to model anisotropy induced by the shear viscosity. We match the interior solution, in noncomoving coordinates, with the Vaidya exterior solution. Two simple models are presented, based on the Schwarzschild and Tolman VI solutions, in the nonadiabatic and adiabatic limit. In both cases, the eventual collapse or expansion of the distribution is mainly controlled by the anisotropy induced by the viscosity.

DOI: 10.1103/PhysRevD.81.104021 PACS numbers: 04.25.−g, 04.25.D−, 04.40.−b

I. INTRODUCTION

In order to study astrophysical fluid dynamics one can get complicated models incorporating realistic transport mechanisms and equations of state. The simplest case with mass, spherical symmetry, despite its simplicity, still remains an interesting problem in numerical relativity, especially when including dissipation. Dissipation due to the emission of massless particles (photons and/or neutrinos) is a characteristic process in the evolution of massive stars. It seems that the only plausible mechanism to carry away the bulk of the binding energy of the collapsing star, leading to a black hole or neutron star, is neutrino emission [1]. Viscosity may be important in the neutrino trapping during gravitational collapse [2–4], which is expected to occur when the central density is of the order 10^{11}–10^{12} g cm^{-3}. Although the mean free path of the neutrinos is much greater than for other particles, the radiative Reynolds number of the trapped neutrinos is nevertheless small at high density [5], rendering viscous the core fluid [1,6].

Numerical relativity is expected to keep its power to solve problems and generate new, interesting physics, when dissipative distributions of matter are considered. In fact, numerical methods in general relativity have been proven to be extremely valuable for the investigation of strong field scenarios (see [7] and references therein). For instance, these methods and frameworks have (i) revealed unexpected phenomena [8], (ii) enabled the simulation of binary black holes (neutron stars) [9,10] and (iii) allowed the development of relativistic hydrodynamic solvers [11], among other achievements. Currently, the main limitation for numerical relativity is the computational demand for three-dimensional evolution [12]. The addition of a test bed for studying dissipation mechanisms and other transport processes in order to later incorporate them into a more sophisticated numerical framework (Arnowitt-Deser-Misner [ADM] or characteristic) is a necessity.

In this paper, we study a self-gravitating spherical distribution of matter containing a dissipative fluid. We follow the method proposed in [13], which introduces a set of conveniently defined "effective" variables (effective pressure and energy density), where their radial dependence is chosen on heuristic grounds. In essence this is equivalent to going one step further from the quasistatic regime, and the method has been named the postquasistatic approximation (PQSA) after [14]. The essence of the PQSA was first proposed in [15] using radiative Bondi coordinates, and it has been extensively used by Herrera and collaborators [16–23]. By quasistatic approximation we mean that the effective variables coincide with the corresponding physical variables (pressure and energy density). However, in Bondi coordinates the notion of quasistatic approximation is not evident: the system goes directly from static to postquasistatic evolution. In an adiabatic and slow evolution we can catch up that phase, clearly seen in noncomov-

[*]Also at the School of Physics, University of Melbourne, Parkville, VIC 3010, Australia
[†]On sabbatical leave from the Universidad de Los Andes while finishing this work.

ing coordinates. This can be achieved using Schwarzschild coordinates [14]. Here, we study radiating viscous fluid spheres in the streaming out limit with the PQSA approach, which allow us to depart from equilibrium in noncomoving coordinates. These systems have been studied using the method described in [15] for the radiative shear viscosity problem and its effect on the relativistic gravitational collapse [24–28]. We do not consider temperature profiles to determine which processes can take place during the collapse. For that purpose, transport equations in the relaxation time approximation have been proposed to avoid pathological behaviors (see for instance [22] and references therein). These issues will be considered in a future investigation. In order to develop a numerical solver that incorporates in a realistic way dissipation following the Müller-Israel-Stewart theory [29–32] it is first necessary to know, to the zeroth level of approximation, viscosity profiles like the ones presented in this investigation. The physical consequences of considering dissipation by means of an appropriate causal procedure have been stated analytically in several papers by Herrera and collaborators (see for example [33–36]).

To the best of our knowledge, no author has undertaken in practice the dissipative matter problem in numerical relativity. Our purpose here is to show how viscosity processes can be considered as anisotropy and how the PQSA works in this context. Our results partially confirm previous investigations [25,26]. The novelty here is in the use of the PQSA to study dissipative scenarios. The results indicate that an observer using radiation coordinates does not ''see'' some details when shear viscosity is considered. The final goal is to eventually study the same problem using the Müller-Israel-Stewart theory for the dissipative system, which is highly nontrivial in spherical symmetry.

In standard numerical relativity, in order to deal with matter both in ADM 3 + 1 [37] and in the characteristic formulations [11], Bondian observers have been used implicitly. This has been noted recently, and the method has been proposed as a test bed in numerical relativity [38]. The systematic use of local Minkowskian and comoving observers in the PQSA, named Bondians, was used to reveal a central equation of state in adiabatic scenarios [39], and to couple matter with radiation [40]. Since Bondian observers are a fundamental part of the PQSA and all its applications in the characteristic formulation, we are currently trying to transfer all the experience gained using this approach to include more realistic effects in the dynamics of the fluid using the ADM 3 + 1 formulation, the most popular method in numerical relativity. Besides introducing a more realistic time scale in the problem with matter, the intention is to promote the PQSA (and any of its applications) as a test bed in the ADM 3 + 1 and characteristic approaches.

This paper is organized as follows: In Sec. II, we present the field equations and matching conditions at the surface of the distribution. We explain the PQSA and write a set of surface equations, in Sec. III. In Sec. IV, we illustrate the method presenting four simple models based on the Schwarzschild and Tolman VI interior solutions. Finally, we discuss the results in Sec. V.

II. FIELD EQUATIONS FOR BONDIAN FRAMES AND MATCHING

To write the Einstein field equations we use the line element in Schwarzschild-like coordinates

$$ds^2 = e^{\nu}dt^2 - e^{\lambda}dr^2 - r^2(d\theta^2 + \sin^2\theta d\phi^2), \tag{1}$$

where $\nu = \nu(t, r)$ and $\lambda = \lambda(t, r)$, with $(t, r, \theta, \phi) \equiv (0, 1, 2, 3)$.

In order to get physical input we introduce the Minkowski coordinates (τ, x, y, z) by [41]

$$\begin{aligned} d\tau &= e^{\nu/2}dt, \qquad dx = e^{\lambda/2}dr, \\ dy &= rd\theta, \qquad dz = r\sin\theta d\phi. \end{aligned} \tag{2}$$

In these expressions ν and λ are constants, because they have only local values.

Next we assume that, for an observer moving relative to these coordinates with velocity ω in the radial (x) direction, the space contains

(i) a viscous fluid of density ρ, pressure $\hat{p}$, effective bulk pressure p_ζ and effective shear pressure p_η, and
(ii) unpolarized radiation of energy density $\hat{\epsilon}$.

For this moving observer, the covariant energy tensor in Minkowski coordinates is thus

$$\begin{pmatrix} \rho + \hat{\epsilon} & -\hat{\epsilon} & 0 & 0 \\ -\hat{\epsilon} & \hat{p} + \hat{\epsilon} - p_\zeta - 2p_\eta & 0 & 0 \\ 0 & 0 & \hat{p} - p_\zeta + p_\eta & 0 \\ 0 & 0 & 0 & \hat{p} - p_\zeta + p_\eta \end{pmatrix}. \tag{3}$$

Note that from (2) the velocity of matter in Schwarzschild coordinates is

$$\frac{dr}{dt} = \omega e^{(\nu-\lambda)/2}. \tag{4}$$

Making a Lorentz boost and defining $\bar{p} \equiv \hat{p} - p_\zeta$, $p_r \equiv \bar{p} - 2p_\eta$, $p_t \equiv \bar{p} + p_\eta$, and $\epsilon \equiv \hat{\epsilon}(1 + \omega)/(1 - \omega)$ we write the field equations in relativistic units $(G = c = 1)$ as follows:

$$\tilde{\rho} = \frac{1}{8\pi r}\left[\frac{1}{r} - e^{-\lambda}\left(\frac{1}{r} - \lambda_{,r}\right)\right], \tag{5}$$

$$\tilde{p} = \frac{1}{8\pi r}\left[e^{-\lambda}\left(\frac{1}{r} + \nu_{,r}\right) - \frac{1}{r}\right], \tag{6}$$

$$p_t = \frac{1}{32\pi}\left\{e^{-\lambda}\left[2\nu_{,rr} + \nu_{,r}^2 - \lambda_{,r}\nu_{,r} + \frac{2}{r}(\nu_{,r} - \lambda_{,r})\right] - e^{-\nu}[2\lambda_{,tt} + \lambda_{,t}(\lambda_{,t} - \nu_{,t})]\right\}, \tag{7}$$

$$S = -\frac{\lambda_{,t}}{8\pi r}e^{-(1/2)(\nu+\lambda)}, \tag{8}$$

where the comma (,) represents partial differentiation with respect to the indicated coordinate and the effective variables $\tilde{\rho}$, S, known as conservation variables as well, and $\tilde{p}$, the flux variable,

$$\tilde{\rho} = \frac{\rho + p_r\omega^2}{1-\omega^2} + \epsilon, \tag{9}$$

$$S = (\rho + p_r)\frac{\omega}{1-\omega^2} + \epsilon \tag{10}$$

and

$$\tilde{p} = \frac{p_r + \rho\omega^2}{1-\omega^2} + \epsilon. \tag{11}$$

Equations (5)–(8) are formally the same as for an anisotropic fluid in the streaming out approximation [26].

At this point, for the sake of completeness, we write the effective viscous pressures in terms of the bulk viscosity ζ, the volume expansion Θ, the shear viscosity η, and the scalar shear σ

$$p_\zeta = \zeta\Theta, \tag{12}$$

$$p_\eta = \frac{2}{\sqrt{3}}\eta\sigma, \tag{13}$$

where

$$\Theta = \frac{1}{(1-\omega^2)^{1/2}}\left[e^{-\nu/2}\left(\frac{\lambda_{,t}}{2} + \frac{\omega\omega_{,t}}{1-\omega^2}\right) + e^{-\lambda/2}\left(\frac{\nu_{,r}}{2}\omega + \frac{1+\omega^2}{1-\omega^2}\omega_{,r} + \frac{2\omega}{r}\right)\right] \tag{14}$$

and

$$\sigma = \pm\sqrt{3}\left(\frac{\Theta}{3} - \frac{e^{-\lambda/2}}{r}\frac{\omega}{\sqrt{1-\omega^2}}\right). \tag{15}$$

We have four field equations for five physical variables (ρ, p_r, ϵ, ω, and p_t) and two geometrical variables (ν and λ). Obviously, we require additional assumptions to handle the problem consistently. However, we discuss first the matching with an exterior solution and the surface equations that govern the dynamics.

We describe the exterior space-time by the Vaidya metric

$$ds^2 = \left(1 - \frac{2\mathcal{M}(u)}{R}\right)du^2 + 2dudR - R^2(d\theta^2 + \sin^2\theta d\phi^2), \tag{16}$$

where u is a timelike coordinate so that $u =$ constant represents, asymptotically, null cones open to the future, and R is a null coordinate ($g_{RR} = 0$). The relationship at the surface between the coordinates (t, r, θ, ϕ) and (u, R, θ, ϕ) is

$$u = t - r - 2\mathcal{M}\ln\left(\frac{r}{2\mathcal{M}} - 1\right), \qquad R = r. \tag{17}$$

The exterior and interior solutions are separated by the surface $r = a(t)$. In order to match both regions on this surface we use the Darmois junction conditions. Demanding the continuity of the first fundamental form, we obtain

$$e^{-\lambda_a} = 1 - \frac{2\mathcal{M}}{R_a} \tag{18}$$

and

$$\nu_a = -\lambda_a. \tag{19}$$

From now on the subscript a indicates that the quantity is evaluated at the surface. Now, instead of writing the junction conditions as usual, we demand the continuity of the first fundamental form and the continuity of the independent components of the energy-momentum flow [42]. This last condition guarantees the absence of singular behaviors on the surface. It is easy to check that

$$\hat{p}_a = p_{\zeta_a} + 2p_{\eta_a}, \tag{20}$$

which expresses the discontinuity of the radial pressure in the presence of viscous processes.

Before proceeding with the description of the method it is convenient to rewrite some equations and introduce one equation of state.

Defining the mass function as

$$e^{-\lambda} = 1 - 2m/r, \tag{21}$$

and substituting (21) into (5) and (8) we obtain, after some arrangements,

$$\frac{dm}{dt} = -4\pi r^2\left[\frac{dr}{dt}p_r + \epsilon(1-\omega)(1-2m/r)^{1/2}e^{\nu/2}\right]. \tag{22}$$

This equation, known as the momentum constraint in the ADM 3 + 1 formulation, expresses the power across any moving spherical shell.

Equation (7) can be written as $T^{\mu}_{1;\mu} = 0$ or equivalently, after a lengthy calculation

$$\tilde{p}_{,r} + \frac{(\tilde{\rho} + \tilde{p})(4\pi r^3 \tilde{p} + m)}{r(r-2m)} + \frac{2}{r}(\tilde{p} - p_t) = \frac{e^{-\nu}}{4\pi r(r-2m)}\left(m_{,tt} + \frac{3m_{,t}^2}{r-2m} - \frac{m_{,t}\nu_{,t}}{2}\right). \quad (23)$$

This last equation corresponds to a generalization of the hydrostatic support equation, that is, the Tolman-Oppenheimer-Volkoff equation. It can be shown that Eq. (23) is equivalent to the equation of motion for the fluid in conservative form in the standard ADM 3 + 1 formulation [38]. Equation (23) leads to the third equation at the surface (see next section); up to this point is completely general within spherical symmetry.

To close this section we have to mention that we assume the following equation of state [26] for nonadiabatic modeling [43]:

$$p_t - p_r = \frac{C(\tilde{p} + \tilde{\rho})(4\pi r^3 \tilde{p} + m)}{(r-2m)}, \quad (24)$$

where C is a constant.

III. THE POSTQUASISTATIC APPROXIMATION AND THE SURFACE EQUATIONS

Feeding back (9) and (11) and using (21) into (5) and (6), these two field equations may be formally integrated to obtain

$$m = \int_0^r 4\pi r^2 \tilde{\rho} dr, \quad (25)$$

which is the Hamiltonian constraint in the ADM 3 + 1 formulation and

$$\nu = \nu_a + \int_a^r \frac{2(4\pi r^3 \tilde{p} + m)}{r(r-2m)} dr, \quad (26)$$

the polar slicing condition, from where it is obvious that for a given radial dependence of the effective variables, the radial dependence of the metric functions becomes completely determined.

As defined in [14] the postquasistatic regime is a system out of equilibrium (or quasiequilibrium; see [34]) but whose effective variables share the same radial dependence as the corresponding physical variables in the state of equilibrium (or quasiequilibrium). Alternatively, we can say that the system in the postquasistatic regime is characterized by metric functions of the static (quasistatic) regime. The rationale behind this definition is not difficult to catch: we look for a regime which, although out of equilibrium, it is the closest to quasistatic evolution.

A. The PQSA protocol

We outline here the PQSA approach:

(1) Take an interior solution to Einstein's field equations, representing a fluid distribution of matter in equilibrium, with static solutions
$$\rho_{\rm st} = \rho(r), \qquad p_{\rm st} = p(r).$$
(2) Assume that the r dependence of $\tilde{\rho}$ and $\tilde{p}$ is the same as that of $\rho_{\rm st}$ and $p_{\rm st}$, respectively.
(3) Using Eqs. (25) and (26), with the r dependence of $\tilde{p}$ and $\tilde{\rho}$, one gets m and ν up to some functions of t, which will be specified below.
(4) For these functions of t one has three ordinary differential equations (hereafter referred to as the surface equations), namely,
(a) Equation (4) evaluated at $r = a$;
(b) Equation (22) evaluated at $r = a$;
(c) Equation $T^{\nu}_{1;\nu} = 0$ evaluated at $r = a$.
(5) Depending on the kind of matter under consideration, the system of surface equations described above may be closed with the additional information provided by the transport equation and/or the equation of state for the anisotropic pressure and/or eventual additional information about some of the physical variables evaluated on the surface of the boundary (e.g. the luminosity).
(6) Once the system of surface equations is closed, it can be integrated for any initial data.
(7) Feeding back the result of integration in the expressions for m and ν, these two functions are completely determined.
(8) With the input from point 7, and using the field equations, together with the equation of state and/or transport equation, all physical variables can be found everywhere inside the matter distribution.

As it should be clear from the above, the crucial point in the algorithm is the system of equations at the surface of the distribution. We specify it in the next section.

B. Surface equations

Evaluating (22) at the surface and using the boundary condition (20), the energy loss is given by

$$\dot{m}_a = -4\pi a^2 \epsilon_a (1 - 2m_a/a)(1 - \omega_a). \quad (27)$$

Hereafter, the overdot indicates d/dt and the a subscript indicates that quantity is evaluated at the surface $r = a(t)$.

The evolution of the boundary is governed by Eq. (4) evaluated at the surface

$$\dot{a} = (1 - 2m_a/a)\omega_a. \quad (28)$$

Scaling the total mass m_a, the radius a and the timelike coordinate by the initial mass $m_a(t=0) \equiv m_a(0)$,

$$A \equiv a/m_a(0), \qquad M \equiv m_a/m_a(0), \qquad t/m_a(0) \to t,$$

and defining

$$F \equiv 1 - \frac{2M}{A}, \quad (29)$$

$$\Omega \equiv \omega_a, \tag{30}$$

$$E \equiv 4\pi a^2 \epsilon_a (1-\Omega), \tag{31}$$

the surface equations can be written as

$$\dot{A} = F\Omega, \tag{32}$$

$$\dot{F} = \frac{F}{A}[(1-F)\Omega + 2E]. \tag{33}$$

Equations (32) and (33) are general within spherical symmetry.

We need a third surface equation to specify the dynamics completely for any set of initial conditions and a given luminosity profile $E(t)$. For this purpose we can use the field Eq. (7) or the conservation Eq. (23), written in terms of the effective variables, which is clearly model dependent.

IV. EXAMPLES

We illustrate the PQSA method with four examples based on the Schwarzschild and Tolman VI interior solutions. Additionally, we consider two corresponding adiabatic models, that is, without free-streaming but anisotropic (viscous). Although greatly simplified, the adiabatic models lead to nontrivial results, which allow to understand our results better.

A. Schwarzschild-like model I: nonadiabatic

We consider here a very simple model inspired by the well-known Schwarzschild interior solution [44]. We take

$$\tilde{\rho} = f(t), \tag{34}$$

where f is an arbitrary function of t. The expression for $\tilde{p}$ is

$$\frac{\tilde{p} + \frac{1}{3}\tilde{\rho}}{\tilde{p} + \tilde{\rho}} = \left(1 - \frac{8\pi}{3}\tilde{\rho} r^2\right)^{h/2} k(t), \tag{35}$$

where k is a function of t to be defined from the boundary condition (20), which now reads, in terms of the effective variables, as

$$\tilde{p}_a = \tilde{\rho}_a \Omega^2 + \hat{\epsilon}_a (1+\Omega)^2. \tag{36}$$

Thus, (35) and (36) give

$$\tilde{\rho} = \frac{3(1-F)}{8\pi a^2}, \tag{37}$$

$$\tilde{p} = \frac{\tilde{\rho}}{3}\left\{\frac{\chi_S F^{h/2} - 3\psi_S \xi}{\psi_S \xi - \chi_S F^{h/2}}\right\}, \tag{38}$$

with

$$\xi = [1 - (1-F)(r/a)^2]^{h/2},$$

where $h = 1 - 2C$ and

$$\chi_S = 3(\Omega^2+1)(1-F) + 2E(1+\Omega),$$
$$\psi_S = (3\Omega^2+1)(1-F) + 2E(1+\Omega).$$

Using (21) and (26) it is easy to obtain expressions for m and ν:

$$m = m_a (r/a)^3, \tag{39}$$

$$e^{\nu} = \left\{\frac{\chi_S F^{h/2} - \psi_S \xi}{2(1-F)}\right\}^{2/h}. \tag{40}$$

In order to write down explicitly the surface equations for this example, we evaluate the Eq. (23) at the surface, obtaining

$$\begin{aligned}\dot{\Omega} = [&8EF - \Omega^2 + 10\Omega^2 F - 6E\Omega + 2E\Omega^2 + 3\Omega^4 \\ &- 8E^2 - 9\Omega^2 F^2 - 6\Omega^4 F + 8E\Omega^3 + 3F^2\Omega^4 \\ &+ 4E^2\Omega + 4E^2\Omega^2 + 4\dot{E}A + 6FE\Omega - 2F\Omega^2 E \\ &- 8F\Omega^3 E)/(2A(F-1)).\end{aligned} \tag{41}$$

It is interesting to note that this equation is the same as in the isotropic case ($p_r = p_t$). This is a direct consequence of the chosen equation of state combined with incompressibility of the fluid; it is not a general result, as we will see for the next models. Equation (41), together with (32) and (33), constitute the system of differential equations at the surface for this model. It is necessary to specify one the luminosity as a function of t and the initial data. We choose E to be a Gaussian

$$E = E_0 e^{-(t-t_0)^2/\Sigma^2},$$

with $E_0 = M_r/\sqrt{\Sigma\pi}$, $t_0 = 5.0$ and $\Sigma = 0.25$, which corresponds to a pulse radiating away $M_r = 1/10$ of the initial mass.

We solve Eqs. (32), (33), and (41) using a fourth order Runge-Kutta method. The physical variables $(\rho, p, \omega, \eta, \epsilon)$ are obtained from the field Eqs. (5)–(8) and the equation of state (24). Note that we have to use Eqs. (14) and (15) and some additional numerical work to determine η. We take as initial conditions $A(0) = 5$, $M(0) = 1$, $\Omega(0) = -0.1$, with $h = 0.99$.

Figure 1 shows the evolution of the radius of the distribution. Figures 2–6 display the physical variables $(\rho, p_r, p_t, \omega, \epsilon)$, Figs. 7 and 8 the kinematic variables Θ and σ, and Fig. 9 the shear viscosity η, for different regions. It is evident that the emission of energy decreases the energy density and the shear viscosity, but increases the pressure; while the collapse is briefly accelerated. It is interesting to note that after the Gaussian emission the distribution recovers staticity slowly, probably in a quasistatic regime. In this model $p_t > p_r$, which means $2\sqrt{3}\sigma\eta > 0$ ($h = 0.99$). It is important to mention that in this model, a shear viscosity $\eta > 0$ is only possible if we choose the negative root in (15). Physically meaningful values of shear viscosity ($\eta > 0$) are obtained for regions

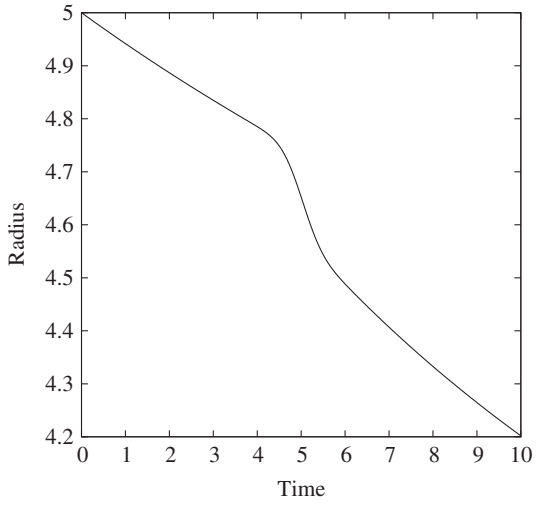

FIG. 1. Evolution of the radius $A(t)$ for the Schwarzschild-like model I. The initial conditions are $A(0) = 5.0$, $F(0) = 0.6$, $\Omega(0) = -0.1$.

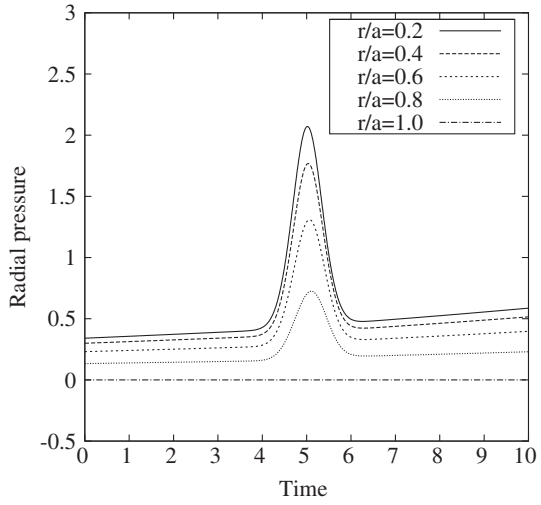

FIG. 3. Evolution of the radial pressure p_r (multiplied by 10^3) for the Schwarzschild-like model I. The initial conditions are $A(0) = 5.0$, $F(0) = 0.6$, $\Omega(0) = -0.1$, with $h = 0.99$.

$r/a \approx 0.6 \rightarrow 1$. This means that the inner core is not viscous but anisotropic. The rest of the kinematic variables (Θ and σ), shown in Figs. 7 and 8, follow the evolution of the radius of the distribution, with Θ (σ) decreasing (increasing) faster as the radius decreases at a faster rate for $4 \lesssim t \lesssim 6$.

B. Schwarzschild-like model II: adiabatic

We construct this model with the same effective variables and metric functions as the aforestudied model I, but now the radiation flux is zero everywhere; therefore this model is adiabatic. Obviously we do not need now an equation of state because all physical variables are determined algebraically from the field equations. However some measure of tangential stress at the surface is required to evolve the system. We opt for a tangential pressure equal to the radial pressure just at the surface, $p_t|_a = p_r|_a$. The third surface equation in this case is

$$\dot{\Omega} = -\frac{1}{2A}(4h\Omega^2F - \Omega^2F + hF - 6\Omega^4F + 3h\Omega^4F - F - 3h\Omega^4 - 4h\Omega^2 - 3\Omega^2 + 1 - h + 6\Omega^4). \tag{42}$$

Observe that this expression explicitly depends on the anisotropic parameter h. In this case we integrate the system for the initial conditions $A(0) = 5$, $M(0) = 1$ and $\Omega = -0.01$. Figure 10 shows the radius of the distribution for different values of h. Figures 11 and 12 display the

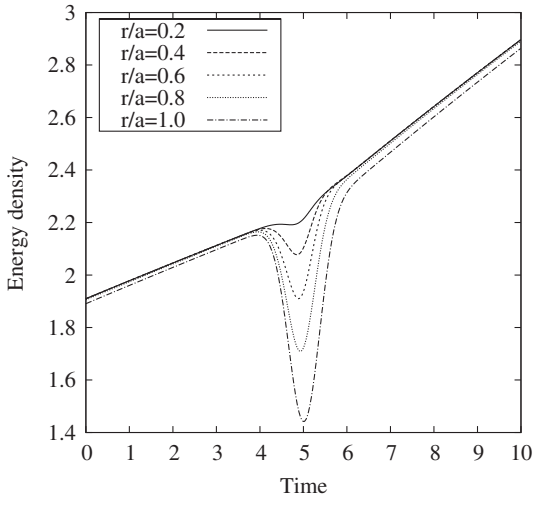

FIG. 2. Evolution of the energy density ρ (multiplied by 10^3) for the Schwarzschild-like model I. The initial conditions are $A(0) = 5.0$, $F(0) = 0.6$, $\Omega(0) = -0.1$, with $h = 0.99$.

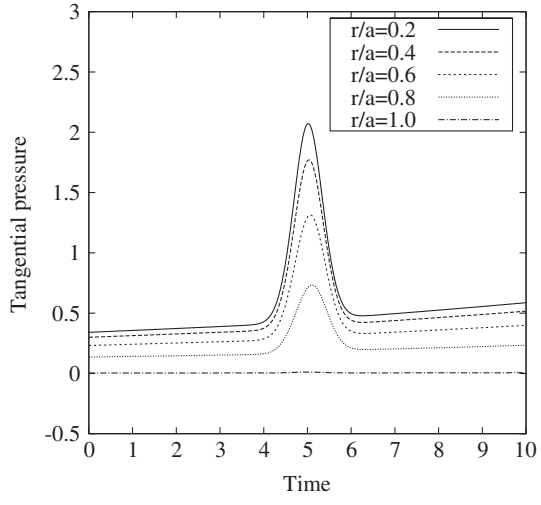

FIG. 4. Evolution of the tangential pressure p_t (multiplied by 10^3) for the Schwarzschild-like model I. The initial conditions are $A(0) = 5.0$, $F(0) = 0.6$, $\Omega(0) = -0.1$, with $h = 0.99$.

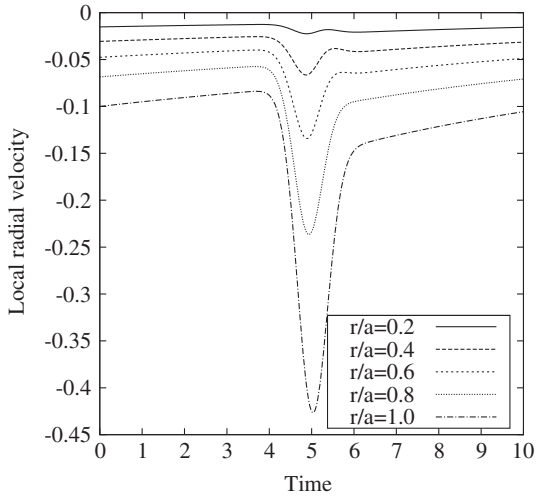

FIG. 5. Evolution of the local velocity ω for the Schwarzschild-like model I. The initial conditions are $A(0) = 5.0$, $F(0) = 0.6$, $\Omega(0) = -0.1$, with $h = 0.99$.

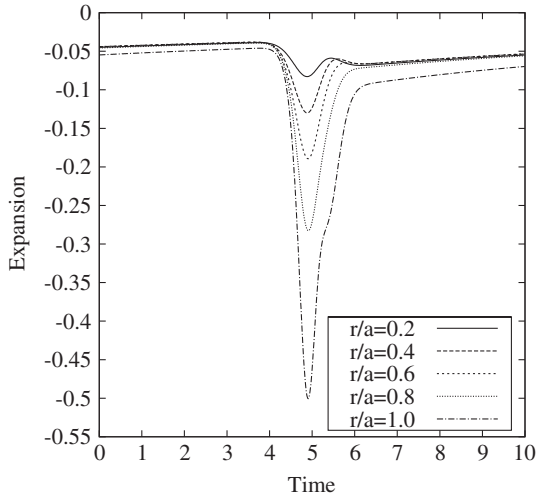

FIG. 7. Evolution of the expansion Θ for the Schwarzschild-like model I. The initial conditions are $A(0) = 5.0$, $F(0) = 0.6$, $\Omega(0) = -0.1$, and $h = 0.99$.

radial velocity and the shear viscosity for $h = 0.9$. In this case anisotropy manifests clearly at the surface. As long as p_t is greater than p_r the collapse accelerates. The same occurs for $0.7 \leq h \leq 1.0$, as we go deeper in the distribution the inner shells collapse faster. The effective gravitation is therefore enhanced by the anisotropy induced by the viscosity. Inner regions have a greater shear viscosity in this model ($\sim$ 10–10^5 times the values found in model I).

C. Tolman VI-like model III: nonadiabatic

In this subsection we revise the model obtained from Tolman's solution VI [45]. Let us take

$$\bar{\rho} = \frac{g}{r^2}, \tag{43}$$

$$\tilde{p} = \frac{gK(1 - 9\alpha(r/a)^{\sqrt{4-3h}})}{3(K/I - 9\alpha(r/a)^{\sqrt{4-3h}})hr^2}, \tag{44}$$

where K and I are defined as

$$K = 8 - 3h + 4\sqrt{4 - 3h}, \qquad I = 8 - 3h - 4\sqrt{4 - 3h}.$$

g and α are functions of t, which can be determined using (36). Therefore,

$$g = \frac{3(1 - F)}{24\pi}, \tag{45}$$

$$\alpha = \frac{3h(1 - F) - K\beta}{9[3h(1 - F) - I\beta]}, \tag{46}$$

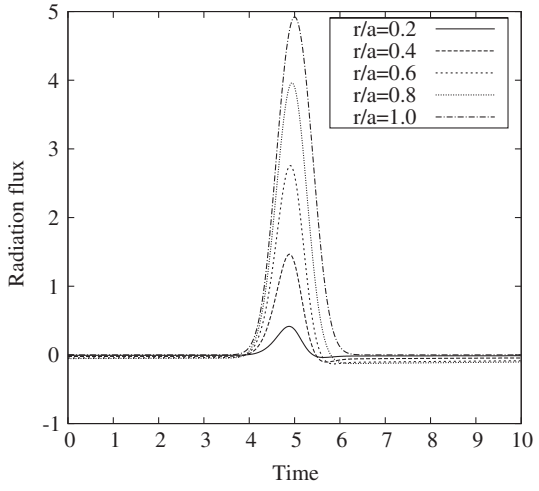

FIG. 6. Evolution of the radiation flux ϵ (multiplied by 10^4) for the Schwarzschild-like model I. The initial conditions are $A(0) = 5.0$, $F(0) = 0.6$, $\Omega(0) = -0.1$, with $h = 0.99$.

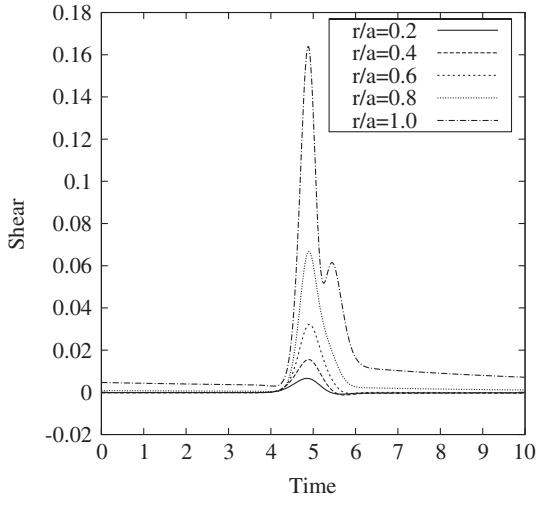

FIG. 8. Evolution of the shear σ for the Schwarzschild-like model I. The initial conditions are $A(0) = 5.0$, $F(0) = 0.6$, $\Omega(0) = -0.1$, and $h = 0.99$.

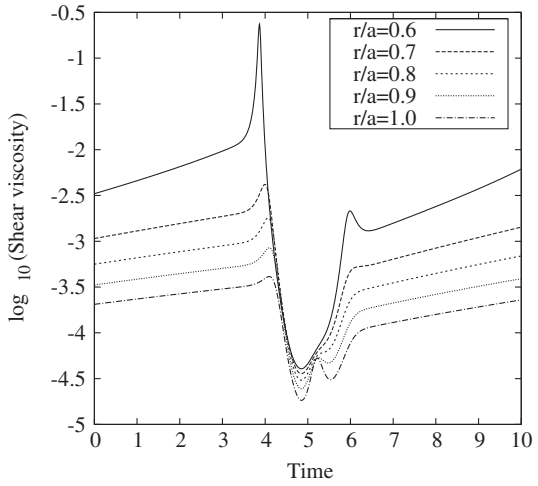

FIG. 9. Evolution of the shear viscosity η for the Schwarzschild-like model I. The initial conditions are $A(0) = 5.0$, $F(0) = 0.6$, $\Omega(0) = -0.1$, with $h = 0.99$.

where

$$\beta = (1 - F)\Omega^2 + 2E(1 + \Omega).$$

Using (21) and (26) we obtain

$$m = m_a(r/a) \tag{47}$$

and

$$\nu = \ln F + \frac{8\pi g}{F}\left(1 + \frac{I}{3h}\right)\ln(r/a) + \frac{8\pi g}{3hF\sqrt{4 - 3h}} \times \left\{I \ln\left(\frac{(K/I - 9\alpha)a^{\sqrt{4-3h}}}{(K/I)a^{\sqrt{4-3h}} - 9\alpha r^{\sqrt{4-3h}}}\right) + K \ln\left(\frac{(K/I)a^{\sqrt{4-3h}} - 9\alpha r^{\sqrt{4-3h}}}{a^{\sqrt{4-3h}}(K/I - 9\alpha)}\right)\right\}. \tag{48}$$

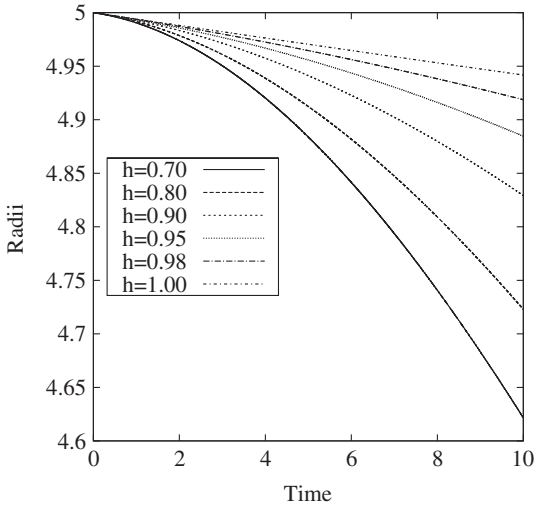

FIG. 10. Evolution of the radius $A(t)$ for the Schwarzschild-like model II. The initial conditions are $A(0) = 5$, $F(0) = 0.6$, $\Omega(0) = -0.01$.

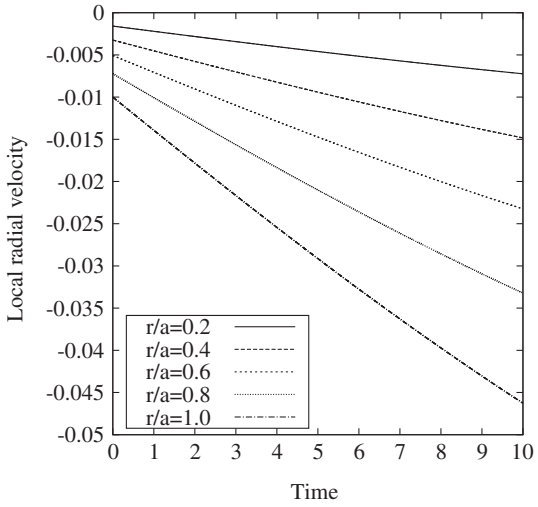

FIG. 11. Evolution of the local radial velocity ω for the Schwarzschild-like model II. The initial conditions are $A(0) = 5$, $F(0) = 0.6$, $\Omega(0) = -0.01$, and $h = 0.9$.

Evaluating Eq. (23) at the surface we can obtain an equation for $\dot{\Omega}$ (too long to display here).

Integrating the system of equations at the surface for the initial conditions $A(0) = 8$ and $\Omega = -0.1$, with $M_r = 10^{-2}$, we obtain Figs. 13–15. We obtain similar results as in model II but in a different fashion. The bigger the difference between the tangential (viscous) pressure p_t and the radial pressure p_r (as h decreases), the more violently the distribution explodes. It is striking that now *all* the spherical shells tend to reach the same instantaneous local radial velocity when the system goes to faster collapse with emission of energy across de boundary surface. At least locally, the ''acceleration'' of all the shells goes to zero at the same time; again the same instantaneous local

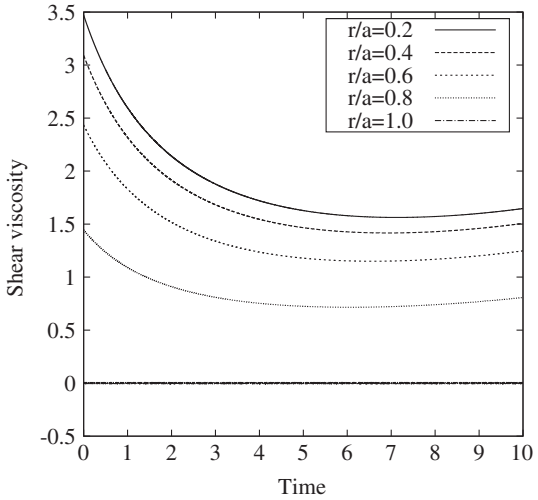

FIG. 12. Evolution of the shear viscosity η (multiplied by 10^2) for the Schwarzschild-like model II. The initial conditions are $A(0) = 5$, $F(0) = 0.6$, $\Omega(0) = -0.01$, and $h = 0.9$.

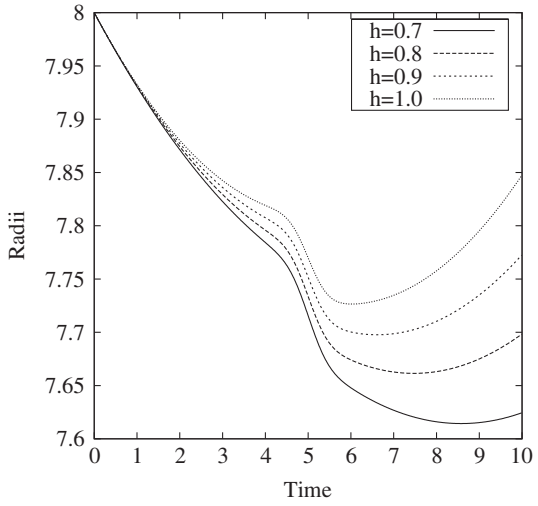

FIG. 13. Evolution of the radii for the Tolman VI-like model III. The initial conditions are $A(0) = 8.0$, $F(0) = 0.75$, $\Omega(0) = -0.1$.

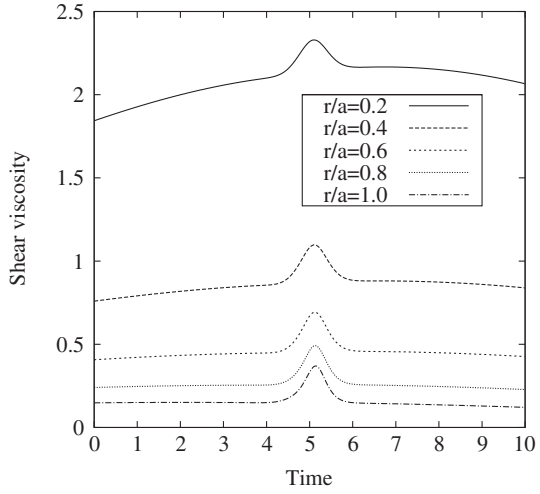

FIG. 15. Evolution of the shear viscosity η (multiplied by 10^4) for the Tolman VI-like model III. The initial conditions are $A(0) = 8$, $F(0) = 0.75$, $\Omega(0) = -0.1$, with $h = 0.95$.

radial velocity (negative) is reached before a final bouncing per shell from outer to inner.

D. Tolman VI-like model IV: adiabatic

We construct this model with the same effective variables and metric functions as in model III, but now the radiation flux is zero everywhere; therefore, this model is adiabatic. Obviously we do not need now an equation of state because all physical variables are determined algebraically from the field equations. However, some measure of tangential stress at the surface is required to evolve the system. We opt for a tangential pressure equal to the radial pressure just at the surface, $p_t|_a = p_r|_a$, as in model II. The third surface equation in this case is

$$\begin{aligned}\dot{\Omega} = (&-9\Omega^4 K h^2 I^2 F + \Omega^4 F I^2 K^3 + 9\Omega^4 K^2 h^2 I F \\ &+ 6\Omega^4 F I^2 K^2 h\sqrt{4-3h} - 243 F I h^4 \Omega^2 - I^3 K^2 F \Omega^4 \\ &- 81 F h^4 I + 54 F I K h^3 \sqrt{4-3h} + 243 K h^4 \Omega^2 F \\ &- 18\Omega^2 F I^2 K h^2 \sqrt{4-3h} - 18\Omega^2 F I K^2 h^2 \sqrt{4-3h} \\ &+ 81 F h^4 K - 18 h^2 I^2 F K \Omega^2 + 18 F h^2 K^2 \Omega^2 I \\ &+ 9\Omega^4 K h^2 I^2 - 9\Omega^4 K^2 h^2 I - 18 h^2 K^2 \Omega^2 I \\ &+ 18 h^2 I^2 K \Omega^2 + I^3 K^2 \Omega^4 - 81 h^4 K - I^2 \Omega^4 K^3 \\ &+ 81 h^4 I + 81 K h^4 \Omega^2 - 81 I h^4 \Omega^2)/[162(K-I) h^4 A].\end{aligned} \tag{49}$$

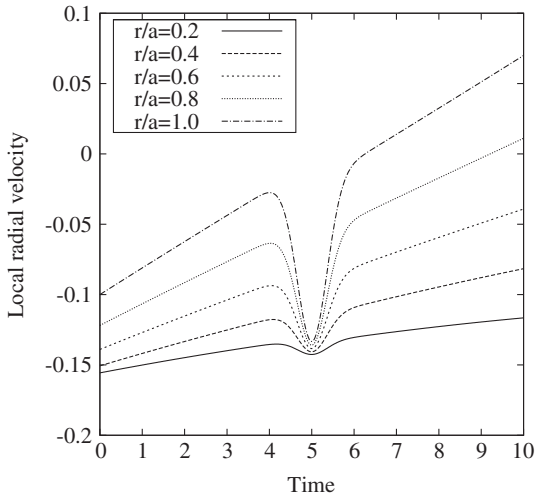

FIG. 14. Evolution of the local radial velocity ω for the Tolman VI-like model III The initial conditions are $A(0) = 8.0$, $F(0) = 0.75$, $\Omega(0) = -0.1$, with $h = 0.95$.

Integrating the system for the initial conditions $A(0) = 8$ and $\Omega = -0.1$, Fig. 13 shows the radius of the distribution for different values of h. Figures 16–18 display the radial velocity and the shear viscosity for $h = 0.9$. After some numerical experimentation some nontrivial results arise, and we relax the condition $p_t > p_r$. At the surface we do not find any novelty. The most violent explosion occurs as $p_r \gg p_t$. In this adiabatic but viscous (anisotropic) model all the shells bounce at the same time to irrupt from inner regions to outer regions with an apparently linear dependence with time. The outer shells of matter are ejected faster and earlier than the inner ones. This sort of behavior was reported several years ago studying in Bondi coordinates the collapse of radiating distributions with an extreme transport mechanism as diffusion [46]. However, the shear viscosity profiles indicate that i) bouncing is not allowed at all and ii) some inner regions are forbidden, otherwise the shear viscosity profiles become negative or/and infinite (see Fig. 18). This situation is general and independent of the anisotropy parameter h.

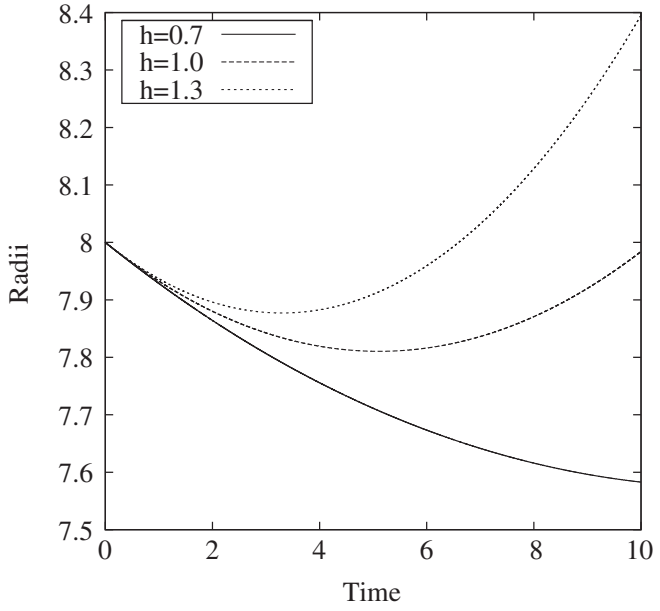

FIG. 16. Evolution of the radii for the Tolman VI-like model IV. The initial conditions are $A(0) = 8.0$, $F(0) = 0.75$, $\Omega(0) = -0.1$.

V. CONCLUSIONS

We consider a self-gravitating spherical distribution of matter containing a dissipative fluid. The use of the PQSA with noncomoving coordinates allow us to study viscous fluid spheres in the streaming out limit as they just depart from equilibrium. From this point of view, the PQSA can also be seen as a nonlinear perturbative method to test the stability of solutions in equilibrium.

For the nonadiabatic Schwarzschild model the distribution evolves to a final state with a nonviscous and anisotropic inner core. Surprisingly, in this model the evolution of the local radial velocity at the surface is the same in the isotropic ($p_t = p_r$) case, a fortuitous coincidence due to the chosen equation and state and the incompressibility of the fluid. For the adiabatic Schwarzschild model the final core is up to 10^5 times more viscous, and the anisotropy appears explicitly in all the evolution equations. The higher viscosity of the core increases the effective gravity and the collapse is faster, as long as $p_t > p_r$.

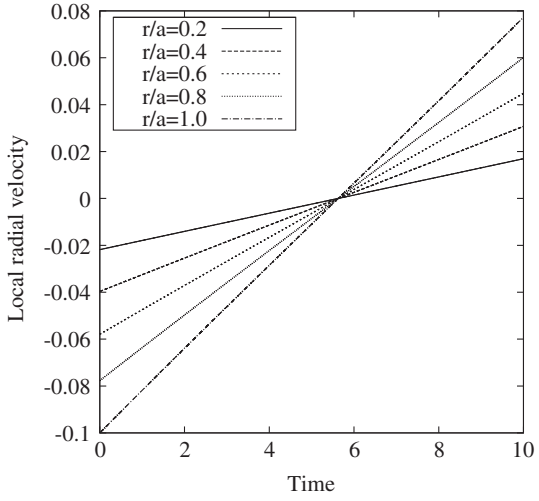

FIG. 17. Evolution of the local radial velocity ω for the Tolman VI-like model IV. The initial conditions are $A(0) = 8.0$, $F(0) = 0.75$, $\Omega(0) = -0.1$, with $h = 0.95$.

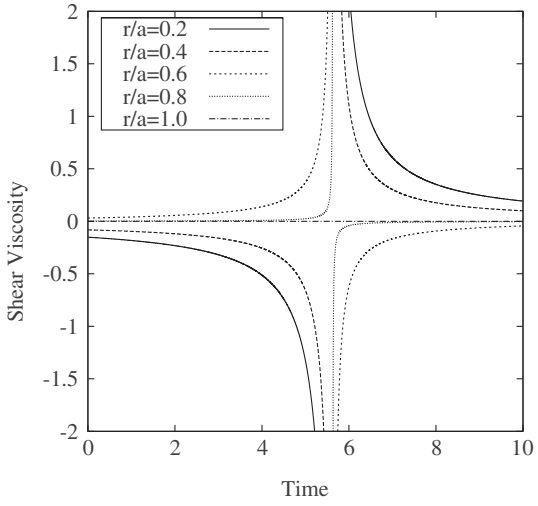

FIG. 18. Evolution of the shear viscosity η for the Tolman VI-like model IV. The initial conditions are $A(0) = 8$, $F(0) = 0.75$, $\Omega(0) = -0.1$, with $h = 0.95$.

Both of the Tolman VI models lead to a distribution which initially collapses and then bounces and expands indefinitely. The Tolman VI nonadiabatic model shares some of the characteristics of the adiabatic Schwarzschild. Before the final bouncing, as $p_t > p_r$ the collapse is accelerated. For the nonadiabatic case some regions of the parameter space are forbidden, since the shear viscosity profiles become unphysical. In this case the bouncing is not allowed and the distribution collapses indefinitely.

A forthcoming paper considers the dissipation by heat flow, in order to isolate effects similar to the ones studied in the present investigation, but with different mechanisms. Also, a work in progress considers heat flow and anisotropy induced by electric charge, pointing to the most realistic numeric modeling in this area [47]. Although they are not entirely new, the results presented here constitute a first cut to more general situations using the PQSA, including dissipation, anisotropy, electric charge, heat flow, viscosity, radiation flux, superficial tension, temperature profiles and study their influence on the gravitational collapse. This investigation is an essential part of a long-term project which tries to incorporate the Müller-Israel-Stewart theory for dissipation and deviations from spherical symmetry, specially when considering electrically charged distributions. Besides being interesting in their own right, we

believe that spherically symmetric fluid models are useful as a test bed for more general solvers in numerical relativity [39,40]. A general three-dimensional code must be able to reproduce situations closer to equilibrium.

ACKNOWLEDGMENTS

C. P. acknowledges the computing resources provided by the Victorian Partnership for Advanced Computation (VPAC).

[1] D. Kazanas and D. N. Schramm, in *Sources of Gravitational Radiation: Proceedings of the Battelle Seattle Workshop, Seattle, Washington, July 24-August 4, 1978*, edited by L. L. Smarr (Cambridge University Press, Cambridge, UK, and New York, 1979), p. 345.
[2] W. D. Arnett, Astrophys. J. **218**, 815 (1977).
[3] G. E. Brown, in *Supernovae: A Survey of Current Research; Proceedings of the Advanced Study Institute, Cambridge, England, June 29-July 10, 1981*, edited by M. J. Rees and R. J. Stoneham (D. Reidel Publishing Company, Dordrecht, The Netherlands, 1982), p. 13.
[4] H. A. Bethe, in *Supernovae: A Survey of Current Research; Proceedings of the Advanced Study Institute, Cambridge, England, June 29-July 10, 1981*, edited by M. J. Rees and R. J. Stoneham (D. Reidel Publishing Company, Dordrecht, The Netherlands, 1982), p. 35.
[5] D. Mihalas and B. Weibel Mihalas, *Foundations of Radiation Hydrodynamics* (Oxford University Press, New York, 1984).
[6] D. Kazanas, Astrophys. J., Lett. Ed. **222**, L109 (1978).
[7] L. Lehner, Classical Quantum Gravity **18**, R25 (2001).
[8] M. W. Choptuik, Phys. Rev. Lett. **70**, 9 (1993).
[9] F. Pretorius, Phys. Rev. Lett. **95**, 121101 (2005).
[10] L. Baiotti, B. Giacomazzo, and L. Rezzolla, Phys. Rev. D **78**, 084033 (2008).
[11] J. A. Font, Living Rev. Relativity **6**, 4 (2003).
[12] J. Winicour, Living Rev. Relativity **12**, 3 (2009).
[13] W. Barreto, B. Rodríguez, and H. Martínez, Astrophys. Space Sci. **282**, 581 (2002).
[14] L. Herrera, W. Barreto, A. Di Prisco, and N. O. Santos, Phys. Rev. D **65**, 104004 (2002).
[15] L. Herrera, J. Jiménez, and G. J. Ruggeri, Phys. Rev. D **22**, 2305 (1980).
[16] L. Herrera and L. A. Nuñez, Fundam. Cosm. Phys. **14**, 235 (1990).
[17] W. Barreto and L. A. Nuñez, Astrophys. Space Sci. **178**, 261 (1991).
[18] W. Barreto, L. Herrera, and L. Nuñez, Astrophys. J. **375**, 663 (1991).
[19] W. Barreto, L. Herrera, and N. Santos, Astrophys. Space Sci. **187**, 271 (1992).
[20] R. Aquilano, W. Barreto, and L. A. Nuñez, Gen. Relativ. Gravit. **26**, 537 (1994).
[21] L. Herrera, A. Melfo, L. A. Nuñez, and A. Patino, Astrophys. J. **421**, 677 (1994).
[22] J. Martínez, Phys. Rev. D **53**, 6921 (1996).
[23] W. Barreto and A. da Silva, Gen. Relativ. Gravit. **28**, 735 (1996).
[24] L. Herrera, J. Jiménez, and W. Barreto, Can. J. Phys. **67**, 855 (1989).
[25] W. Barreto and S. Rojas, Astrophys. Space Sci. **193**, 201 (1992).
[26] W. Barreto, Astrophys. Space Sci. **201**, 191 (1993).
[27] W. Barreto and L. Castillo, J. Math. Phys. (N.Y.) **36**, 5789 (1995).
[28] W. Barreto, J. Ovalle, and B. Rodríguez, Gen. Relativ. Gravit. **30**, 15 (1998).
[29] I. Müller, Z. Phys. **198**, 329 (1967).
[30] W. Israel, Ann. Phys. (N.Y.) **100**, 310 (1976).
[31] W. Israel and J. M. Stewart, Phys. Lett. **58A**, 213 (1976).
[32] W. Israel and J. M. Stewart, Ann. Phys. (N.Y.) **118**, 341 (1979).
[33] L. Herrera, A. Di Prisco, J. L. Hernández-Pastora, J. Martín, and J. Martínez, Classical Quantum Gravity **14**, 2239 (1997).
[34] L. Herrera and J. Martínez, J. Math. Phys. (N.Y.) **39**, 3260 (1998).
[35] L. Herrera, A. di Prisco, J. Martin, J. Ospino, N. O. Santos, and O. Troconis, Phys. Rev. D **69**, 084026 (2004).
[36] L. Herrera, A. di Prisco, and W. Barreto, Phys. Rev. D **73**, 024008 (2006).
[37] D. W. Neilsen and M. W. Choptuik, Classical Quantum Gravity **17**, 733 (2000).
[38] W. Barreto, Phys. Rev. D **79**, 107502 (2009).
[39] W. Barreto, L. Castillo, and E. Barrios, Phys. Rev. D **80**, 084007 (2009).
[40] W. Barreto, L. Castillo, and E. Barrios (unpublished).
[41] H. Bondi, Proc. R. Soc. A **281**, 39 (1964).
[42] L. Herrera and A. Di Prisco, Phys. Rev. D **55**, 2044 (1997).
[43] M. Cosenza, L. Herrera, M. Esculpi, and L. Witten, Phys. Rev. D **25**, 2527 (1982).
[44] K. Schwarzschild, Sitzungsber. Preuss. Akad. Wiss. Berlin (Math. Phys.) **1916**, 189, (1916) [Gen. Relativ. Gravit. **35**, 951 (2003)].
[45] R. C. Tolman, Phys. Rev. **55**, 364 (1939).
[46] W. Barreto, L. Herrera, and N. Santos, Astrophys. J. **344**, 158 (1989).
[47] A. Di Prisco, L. Herrera, G. Le Denmat, M. McCallum, and N. Santos, Phys. Rev. D **76**, 064017 (2007).